Application of the density functional method to study adsorption and phase transitions in two-site associating, Lennard-Jones fluids in cylindrical pores

2000 J. Phys.: Condens. Matter 12 8785

(http://iopscience.iop.org/0953-8984/12/41/304)

J. Phys.: Condens. Matter **12** (2000) 8785–8800. Printed in the UK PII: S0953-8984(00)14611-9

Application of the density functional method to study adsorption and phase transitions in two-site associating, Lennard-Jones fluids in cylindrical pores

Beatriz Millan Malo†, Lorena Salazar‡, Stefan Sokolowski§ and Orest Pizio‡‖

† Instituto de Fisica de la UNAM, Coyoacán 04511, México DF
‡ Facultad de Ciencias, Universidad Autonoma de Estado de Mexico, Av. Literario 100, Toluca, Mexico
§ Department for the Modelling of Physico-Chemical Processes, Marie Curie-Skłodowska University, Lublin 200-31, Poland

Received 8 June 2000, in final form 29 August 2000

Abstract. A density functional approach is applied to study the adsorption of an associating model fluid in narrow cylindrical capillaries. The model with non-associative Lennard-Jones (LJ), attraction between fluid particles and the site–site association, permitting the formation of chains of LJ monomers, i.e. the two-site model for monomers, is investigated. The strength of associative interactions is varied in the model to obtain an insight into the role of the associative interactions on the phase diagrams of confined fluids. The fluid–pore walls interaction is chosen in the form of the Yukawa-type potential. The wetting properties of the confining solid surface is studied first. Next, we describe the first-order layering transitions in cylindrical pores and the phenomenon of capillary condensation in capillaries of molecular dimensions. We also analysed the structural changes in the adsorbed fluids accompanying layering transitions and capillary condensation. A comparison of the phase diagrams for the fluid in the cylindrical pores with two different radii and in the slit-like pores, with the same nominal width as the cylindrical pores, is performed. We have also compared the capillary evaporation phase diagram for the model in question in cylindrical and slit-like pores. The method and the results represent a useful basis for the development of inhomogeneous statistical associating fluid theory for several practical applications.

1. Introduction

Several investigations have been concerned with the microscopic structure and thermodynamic properties, including phase transitions, of simple fluids adsorbed in pores of various geometry, see e.g. [1–3] for a comprehensive discussion of the subject.

The properties of fluids confined to pores of molecular dimensions differ from those of the bulk fluid. For example, capillary condensation of a fluid in the pore occurs at a lower value of the chemical potential than the bulk vapour–liquid transition. Also the critical temperature of the capillary condensation of simple fluids is depressed with respect to the bulk critical temperature. In addition, capillary condensation may be preceded by a single or a series of the first-order layering transitions. The structure of the adsorbed fluid differs from the bulk fluid structure.

‖ On sabbatical leave from the Instituto de Quimica de la UNAM.

0953-8984/00/418785+16$30.00

The most popular models for the pore geometry, involved in a large number of studies, have been the slit-like and cylindrical models. In both cases, the pore represents an open system with an infinite surface area. The fluid confined in the open pore must be in equilibrium with an external reservoir at a certain value of the chemical potential for the fluid species. Usually the cylindrical pore geometry is considered to be a more realistic model for real adsorbents. However, cylindrical geometry hinders analytical research, and, moreover, makes the procedure of finding the numerical solutions much more demanding, in comparison to the case of a slit-like pore.

Much less investigated are the properties of confined associating fluids, in contrast to the behaviour of simple fluids. Associating fluids are ubiquitous in nature—water, methanol, hydrofluorocarbons are some of these systems. The studies of homogeneous associating fluids, including their thermodynamics and structural properties, have become popular and really successful after the appearance of the theory of Wertheim for chemical association in the mid 1980s [4–7]. This theory consists of two parts, namely of the Ornstein–Zernike (OZ) type integral equations and of thermodynamic perturbation theory (TPT). Both ingredients have in common that the correlation functions and thermodynamic properties are constructed by using the fugacity expansion for saturable, orientation-dependent, finite-range strong attraction, rather than the commonly used density expansions. The TPT has been applied to a wide set of models of associating fluids, beginning from a simple dimerizing model, in which each of the monomers is characterized by one attractive bonding site, up to sophisticated models with two, three, four and five attractive sites per monomer [8–12]. The model with two sites is useful to consider the formation of chains via the chemical association mechanism, whereas the models with a larger number of sites may serve to consider network-forming fluids. In each of the models studied by using the TPT, the effect of the non-associative attractive LJ-type forces has been taken into account in the mean field approximation. The theory has been very carefully tested with respect to computer simulation data, at the level of the one-, two- and four-site models [8–11], and has been shown to be quite accurate. The TPT applications for simple models have been followed by the construction of the so-called statistical associating fluid theory (SAFT) [13–16]. Two essentials can be attributed to this theoretical approach. Namely, the explicit form of the free energy is chosen according to the specific system of experimental interest and besides, the parameters of the model are fitted, for example, to the experimentally measured critical values (critical temperature and density) or to some low-temperature data or to vapour pressure data in the certain range of temperatures, see e.g. [13–16] for a detailed description. Anyway, the SAFT approach at its present stage of development permits, with reasonable accuracy and with reasonable computational effort, to predict a wide set of thermodynamic properties and phase diagrams for one-component associating fluids and two-component mixtures and represents successful and useful chemical engineering tools.

It seems unnecessary to emphasize that the knowledge of interfacial thermodynamic and structural properties for the model associating fluids would be of much importance both for basic research and for practical applications. However, to describe inhomogeneous associating fluids is not a simple task. It is well known that the method of integral equations in the common theory of liquids faces severe difficulties in describing the thermodynamics of fluids with attractive interparticle interactions as well as in describing the interfacial thermodynamics of simple fluids. Attempts to extend the integral equations of Wertheim's OZ type to the presence of external fields have also been undertaken. These extensions comprise the first-order, or the so-called singlet, integral equations [17, 18], as well as the second-order Wertheim's type OZ equations, or the so-called pair level theory [19, 20]. The structural properties of the inhomogeneous models involving only hard-core type repulsive forces, as well as associative interactions between fluid species, can be described by these tools. However, things become

difficult if the non-associative attractive interactions are included in the models. In particular, by construction, the singlet level integral equations are unable to describe phase transitions in inhomogeneous simple and associating fluids. The pair level theories are formally capable of describing the surface phase transitions, but they require very extensive numerical calculations and have almost vanishing practical usefulness in this respect. Moreover, accuracy of a closure, necessary to complete an integral equation, with respect to the prediction of phase transitions is difficult to establish. As a consequence of these factors, the second-order integral equations are unable to compete with the density functional (DF) methods discussed in great detail in [21, 22]. The DF methods have been implemented with much success to describe the thermodynamic properties and phase transitions in simple fluids near walls and under a variety of microporous confinements, including pores of slit-like shape intervened by geometrical or energetic heterogeneity at the molecular scale, see e.g. [23, 24].

A particular DF approach for fluids with a temperature-dependent association of the species has been proposed by Segura *et al* [25]. Their technique combines a density functional theory for non-associating particles, see e.g. [21, 22], with Wertheim's TPT for chemical association [4–8]. Wertheim's theory has actually been constructed in the form of an associative free energy functional. The success of Wertheim's approach and of the TPT was one of the principal motivations for the development of a similar line of research for inhomogeneous associating fluids. However, Segura *et al* [25, 26] have focused their attention only on the structural properties and thermodynamics of the model for associating hard spheres in contact with a hard wall. It has been shown that the proposed theory is in reasonable agreement with the canonical Monte Carlo simulations of these systems [25–27]. Before our recent publications [27–30], it had not been attempted to include attractive interactions between fluid species, as well as between them and a confining solid surface, and consequently the problem of the surface phase transition had not been addressed.

The associative DF theory has been systematically applied to study the adsorption of associating LJ fluids on solid surfaces [27, 30] and in slit-like pores [28, 29]. The present study is the continuation of our recently published works.

In this work, however, we focus on some new features of the behaviour of confined associating fluids, restricting ourselves, without loss of much generality, to the chain-forming model with two bonding sites per monomer. First, our interest is in the adsorption of this model fluid in pores of cylindrical shape. We have chosen the fluid–pore wall interaction potential similar to previously studied models of the adsorption of simple fluids into cylindrical pores [31, 32]. In the limit of infinite pore radius the fluid–wall potential reduces to the Yukawa-type potential. In the first part of this work we have performed an analysis of the wetting properties of the solid surface in question, with respect to the model associating fluid at two values of association energy between fluid species. Next the phase diagrams of the associating fluid model in capillaries of different width have been calculated in great detail. We consider the first-order layering transitions in the cylindrical capillaries and capillary condensation. In order to obtain an insight into the role of the shape of confinement on capillary condensation, we have performed a comparison of the phase diagrams for the associating fluid model in the cylindrical pores and in the slit-like pores of the width nominally equal to the cylindrical pore diameter, assuming the same fluid–wall interaction potential for both cases. Moreover, we have performed a comparison of the capillary evaporation phase diagrams obtained for the cylindrical and slit-like pore cases. The structural properties of the model in cylindrical pores are discussed in terms of the density profiles of species, of the density profile of unbonded species and of the average chain length in the pore. These properties in conjunction permit us to present a quite comprehensive description of adsorption and phase transitions for the model associating fluid in pores of cylindrical and slit-like geometry.

To conclude the introductory part of this work, our focus is on the adsorption of chain-forming LJ associating fluid in narrow cylindrical pores. The fluid model has been involved in the studies of some n-alkanes and methanol [14]. However, the present formulation of the associative DF theory does not include all the terms of the free energy according to the SAFT treatment of alkanes, for example. Our desire for future research is to combine a complete SAFT free energy expression for the associating model in question, and related models, with another density functional approach more adequate to deal with mixtures of associating monomers belonging to different species. This would result in an understanding of the interfacial behaviour of several systems of practical importance.

The theoretical developments used in this work are similar to those given in [27–30]. However, for the sake of the reader, we repeat principal theoretical arguments quite briefly and, besides, discuss some novel issues relevant to our study.

2. Modelling and theory

Similar to previous work on associating fluids [8], we consider a system of particles interacting via the angular dependent pair potential

$$u(\boldsymbol{r}_{12}, \boldsymbol{\omega}_1, \boldsymbol{\omega}_2) = u_{non}(r_{12}) + \sum_{A} \sum_{A'} u_{AA'}(\boldsymbol{r}_{12}, \boldsymbol{\omega}_1, \boldsymbol{\omega}_2) \tag{1}$$

where r_{12} is the magnitude of the vector $\boldsymbol{r}_{12}$ connecting the centres of molecules 1 and 2, and $\boldsymbol{\omega}_i$, $i = 1, 2$, are the orientations of molecules 1 and 2 relative to the vector $\boldsymbol{r}_{12}$. The non-associative part of the pair energy, $u_{non}(r_{12})$, is given by a truncated LJ potential

$$u_{non}(r) = \begin{cases} \varepsilon[(\sigma/r)^{12} - (\sigma/r)^6] & r < r_{cut} \\ 0 & \text{otherwise} \end{cases} \tag{2}$$

where $r_{cut} = 2.5\sigma$ is the cut-off distance; ε and σ are the parameters of the LJ interaction, that are chosen as the energy and the length units ($\varepsilon = 1$, $\sigma = 1$). The association potential between a site A on the molecule 1 and a site A' on the molecule 2 denoted as $u_{AA'}$, is a square-well attraction with cone shape geometry, similar to previous studies of the bulk associating fluids [8],

$$u_{AA'}(\boldsymbol{r}_{12}, \boldsymbol{\omega}_1, \boldsymbol{\omega}_2) = \begin{cases} -\varepsilon_{AA'} & r_{12} < r_{ca}, \theta_{A1} < \theta_c, \theta_{A'2} < \theta_c \\ 0 & \text{otherwise} \end{cases} \tag{3}$$

where θ_{Xi}, $X = A, A'$, $i = 1, 2$, is the angle between the vector from the centre of molecule i to the site X and the vector $\boldsymbol{r}_{12}$.

In the model for a chain-forming fluid, each molecule has two sites, labelled A and A'. We assume that two molecules can form a bond only via the sites labelled differently, i.e. the bond can form via the A, A' pair, but not via the AA or $A'A'$ pair. In other words $u_{AA} = u_{A'A'} = 0$. The molecules can form chains through the site–site attraction. The square-well attractive energy, $\varepsilon_{AA'}$ is denoted as ε_{as}. The upper limit of the square-well attraction, r_{ca}, is chosen on the surface of LJ fluid particles, i.e. at $r_{ca} = 1$, and the bonding angle is $\theta_c = 27^\circ$.

The fluid particles interact with cylindrical pore walls via the one-dimensional potential $v_c(R)$, that depends only on the radial distance R from the pore centre. We assume that the fluid–wall interaction is in the form of the Yukawa-type potential, similar to previous studies of the adsorption of simple fluids confined to cylindrical capillaries [31, 32]

$$v_c(R) = \begin{cases} \infty & R > R_c \\ -2\varepsilon_{gs}\lambda R_c K_1(\lambda R_c) I_0(\lambda R) & R < R_c \end{cases} \tag{4}$$

with the parameters ε_{gs} and λ; R_c is the radius of the cylindrical capillary. The functions $K_1(x)$ and $I_0(x)$ are modified Bessel functions. The values for the parameters ε_{gs} and λ are chosen to be fixed throughout this study, and equal to 10 and 5, respectively. In the limits $R_c \to \infty$, $R \to \infty$, $z = |R_c - R| \ll R_c$

$$v(R) \to -\varepsilon_{gs} \exp(-\lambda z) \tag{5}$$

such that the cylindrical wall potential reduces to the planar wall potential.

We employ the limiting behaviour given by (5) to investigate the wetting properties of a single solid surface with respect to the associating model in question and in slit-like pores. Moreover, to perform comparisons between the cylindrical pore case and the slit-like pore of the width, H, centred at $R = 0$, with $H = 2R_c$, we model the fluid–slit-like pore potential, $v_{sl}(R)$, as follows,

$$v_{sl}(R) = \begin{cases} \infty & |R| > H/2 \\ v(R) & |R| < H/2 \end{cases} \tag{6}$$

where $v(R)$ is given by (5). After describing the model, we proceed to theoretical issues.

According to usual density functional methodology [21, 22], the theory provides an approximation for the grand thermodynamic potential

$$\Omega = F + \int \rho(\boldsymbol{r})[v(\boldsymbol{r}) - \mu]\,\mathrm{d}\boldsymbol{r} \tag{7}$$

as a functional of the number density of a fluid, $\rho(\boldsymbol{r})$, at a given value of the configurational chemical potential μ; $v(\boldsymbol{r})$ is the external field. The Helmholtz free energy, F, is the sum of an ideal and excess terms, $F = F^{id} + F^{ex}$. The ideal contribution is known exactly. The excess part of the free energy consists of two terms, namely $F^{ex} = F^{ex}_{non} + F^{ex}_{as}$; this decomposition is used in the spirit of the similar decomposition of the fluid–fluid interaction potential in (1).

Several density functional approaches have been developed for fluids interacting via non-associative, LJ interactions. Here we would like to employ the method in which the non-associative attractive forces are considered in the *mean field approximation*, whereas the effects from repulsive forces are taken into account by using the *smoothed density approximation*. To begin with, the non-associative LJ potential, $u_{non}(r_{12})$, is decomposed into the repulsive and the attractive part according to the Weeks–Chandler–Andersen (WCA) scheme [33], $u_{non}(r) = u_{rep}(r) + u_{att}(r)$

$$u_{rep}(r) = \begin{cases} u_{non}(r) + \varepsilon & r \leqslant 2^{1/6}\sigma \\ 0 & r > 2^{1/6}\sigma \end{cases} \qquad u_{att}(r) = \begin{cases} -\varepsilon & r \leqslant 2^{1/6}\sigma \\ u_{non}(r) & r > 2^{1/6}\sigma. \end{cases} \tag{8}$$

Moreover, we assume that the associative contribution to the excess free energy can also be written in terms of the smoothed density approximation, according to the approach proposed by Segura *et al* [25]. The excess free energy under these assumptions has the form

$$F^{ex} = \int \rho(\boldsymbol{r}) f^{ex}_{rep}[\tilde{\rho}(\boldsymbol{r})]\,\mathrm{d}\boldsymbol{r} + \int \rho(\boldsymbol{r}) f^{ex}_{as}[\tilde{\rho}(\boldsymbol{r})]\,\mathrm{d}\boldsymbol{r} + \frac{1}{2}\int \mathrm{d}\boldsymbol{r}_1\,\mathrm{d}\boldsymbol{r}_1\, u_{att}(r_{12})\rho(\boldsymbol{r}_1)\rho(\boldsymbol{r}_2) \tag{9}$$

where f^{ex} in each of the first two terms in the right-hand side of (9) denotes the excess free energy density per particle, in terms of the smoothed density ($\tilde{\rho}$) approximation. It is important to make clear that the decomposition of the non-associative potential according to (8) does not concern the associative, second term in (9).

The smoothed density function is chosen according to the theory of Tarazona [34], see also [21]. Following Tarazona [34], we assume that $f^{ex}_{rep}(\tilde{\rho})$ follows from the Carnahan–Starling equation of state. However, possible optimization of the diameter for effective hard spheres

has been neglected as a secondary effect, the packing fraction of hard spheres in the equation of state has been calculated by using the LJ diameter.

The associative contribution to the free energy is taken from the Wertheim's first-order TPT [4–8], dependent, however, on the smoothed density

$$f_{as}^{ex}(\tilde{\rho})/kT = \sum_{A=1,M} [\ln \chi_A(\tilde{\rho}) - \chi_A(\tilde{\rho})/2 + 0.5]. \tag{10}$$

χ_A is the fraction of fluid molecules *not* bonded at a site A. According to the statistical mechanical analogue of the law of mass action, formally generalized for an inhomogeneous system, the equation for the fraction of particles not bonded at a site A must be evaluated from the equation [25, 35]

$$\chi_A(\boldsymbol{r}_1) = \frac{1}{1 + \sum_{1<A'<N_A} \int \mathrm{d}\boldsymbol{r}_2\, \rho(\boldsymbol{r}_2)\chi_{A'}(\boldsymbol{r}_2)g^{non}(\boldsymbol{r}_1, \boldsymbol{r}_2) f_{AA'}(r_{12})} \tag{11}$$

where N_A ($N_A = 2$) is the number of sites on the second molecule with which the site A on the first molecule is eligible to bond; $f_{AA'}(r_{12}) = \langle \exp[-u_{AA'}(r_{12}, \boldsymbol{\omega}_1, \boldsymbol{\omega}_2)/kT] - 1\rangle_{\Omega_1,\Omega_2}$ is an angle-averaged site–site Mayer function (over the orientations of molecules 1 and 2) and $g^{non}(\boldsymbol{r}_1, \boldsymbol{r}_2)$ is the pair correlation function of the inhomogeneous non-associating fluid. According to the first-order thermodynamic perturbation theory, equation (11) contains only the angular averaged function $f_{AA'}(r_{12})$, such that the orientational effects of bonding cannot be captured in the framework of this theory. Equation (11) is difficult to deal with without some further approximations. They have been discussed by us in more detail in our recent work [28]. In particular, the pair correlation function for an inhomogeneous fluid is approximated by the corresponding function for the *uniform fluid* to evaluate the fraction of unbonded particles [28]. In contrast to our previous work [27–30], we have chosen the bonding distance to be equal to the LJ diameter, similar to modelling employed in the works from Gubbins' group [36–38], such that the previously discussed procedure requires a few additional comments. In essence, we calculate $\chi_A(\boldsymbol{r})$ according to the approximation developed in [25, 27, 28]

$$\chi_A(\boldsymbol{r}) \equiv \chi_A(\tilde{\rho}) = \frac{1}{1 + \sum_{1<A'<N_A} \tilde{\rho}\chi_A(\tilde{\rho})\Delta_{AA'}} \tag{12}$$

where

$$\Delta_{AA'} = \pi(1 - \cos\theta_c)^2(\exp(-\varepsilon_{as}/kT) - 1) \int \mathrm{d}r\, r^2 g_{LJ}(r). \tag{13}$$

However, to evaluate $\Delta_{AA'}$ requires a knowledge of the distribution function for LJ non-associative fluid, $g_{LJ}(r)$. At this stage of the calculations we have employed the procedure thoroughly discussed by Johnson and Gubbins [36] and Walsh and Gubbins [37] and approximate the structure of the LJ fluid by the structure of a softly repulsive fluid

$$g_{LJ}(r) \approx \exp(-u_{rep}(r)/kT) y_d(r) \tag{14}$$

where $y_d(r)$ denotes the cavity correlation function of a fluid of hard spheres with diameter d. The cavity function is obtained by using the Percus–Yevick approximation. It has been shown that the procedure is fairly accurate for the bulk associating fluid model in question, see e.g. [36]. It seems that all the intermediate steps of the procedure have been sufficiently well discussed.

Finally, at equilibrium, $\delta\Omega/\delta\rho(\boldsymbol{r}) = 0$, and hence one needs to solve the equation for the density profile,

$$-kT \ln[\rho(R)] = v(R) + f^{ex}[\tilde{\rho}(R)] - f^{ex}(\rho_b) + \int \frac{\delta\tilde{\rho}(R')}{\delta\rho(R)} f^{ex\prime}[\tilde{\rho}(R')]\rho(R')\,\mathrm{d}\boldsymbol{r}'$$
$$-\rho_b f^{ex'}(\rho_b) + \int u_a(|\boldsymbol{r} - \boldsymbol{r}'|)[\rho(R') - \rho_b]\,\mathrm{d}\boldsymbol{r}' \tag{15}$$

where $f^{ex\prime}$ is the excess free energy derivative with respect to fluid density, and ρ_b is the bulk density, corresponding to the configurational chemical potential μ ($f^{ex} = f^{ex}_{rep} + f^{ex}_{as}$); the external field is taken according to (5), (4) or (6), for the cylindrical pore case, for a single plane substrate and for a slit-like pore, respectively.

3. Results and discussion

The solutions for the density profile equation, (15), were obtained by using a Picard type iterative method. We have performed very demanding calculations along either the increasing or decreasing bulk density branches, taking the final profile obtained at the preceding bulk density as the starting profile to obtain a solution at a new bulk density. The integrals in (15) were evaluated by a trapezoidal rule; a mesh width of 0.025 was found to provide sufficient numerical accuracy. The iterations were continued until the maximum difference between two subsequent profiles was smaller than 10^{-4}. The bulk density, ρ_b and the density profiles, $\rho(R)$ are dimensionless. The definition of the reduced temperature is as usual, $T^* = kT/\varepsilon$.

Once the profile is known, we calculate the excess adsorption isotherm

$$\Gamma = \int \mathrm{d}R\,[\rho(R) - \rho_b] \tag{16}$$

and the excess grand potential per unit area, $\Omega_s = (\Omega - \Omega_b)/A$, where Ω_b is given by (7) with the density equal to the bulk density, ρ_b, with the external field switched off. The locus of a given phase transition has been found by analysing the dependence of the excess grand thermodynamic potential on the configurational chemical potential as explained in [27, 28].

However, before proceeding to the results obtained for adsorption in pores, we would like to characterize the wetting properties of the solid constituting the pore walls. To do that we consider the two-site associating LJ model fluid in question in contact with single planar solid surface. The interaction potential between fluid particles and the confining surface is given by (5). The model fluid is studied at two values of the association energy, namely $\varepsilon_{as} = 8$ (a weakly associating fluid) and $\varepsilon_{as} = 20$ (a strongly associating fluid). This first case is referred to as a weakly associating fluid because the critical temperature of the *bulk* associating model, T_c^*, in this case is $\approx$1.41, such that the difference between the critical temperature of the LJ model with truncated potential ($T_c^* \approx 1.32$) is quite small. The critical temperatures of the two aforementioned models have been evaluated within the *bulk* counterpart of the theory of this study employing the same numerical algorithm and accuracy. On the other hand, the critical temperature of the model with $\varepsilon_{as} = 20$ is $T_c^* \approx 2.41$—which differs very much from the non-associative LJ model. Therefore, according to physical intuition: higher association energy—higher critical temperature of the model, we refer to the model with $\varepsilon_{as} = 20$ as a strongly associating model. However, this qualitative definition does not clarify any issue concerning interfacial criticality, before performing a detailed investigation.

3.1. Two-site associating LJ model fluid in contact with a solid surface

For illustrative purposes we present fragments of adsorption isotherms for a weakly associating model in figures 1(a) and 1(b). The curves given in figure 1(a) concern a low density part of the isotherms in terms of Γ dependent on the density normalized by the density for vapour–liquid transition for the bulk fluid (ρ_s) at the temperature in question. The second fragment of the first figure (figure 1(b)) concerns a high-density part of the same adsorption isotherms. We observe that at a high temperature the adsorption is continuous, whereas a set of transitions can be observed at lower temperatures. Figure 1(a) describes the appearance and evolution of the

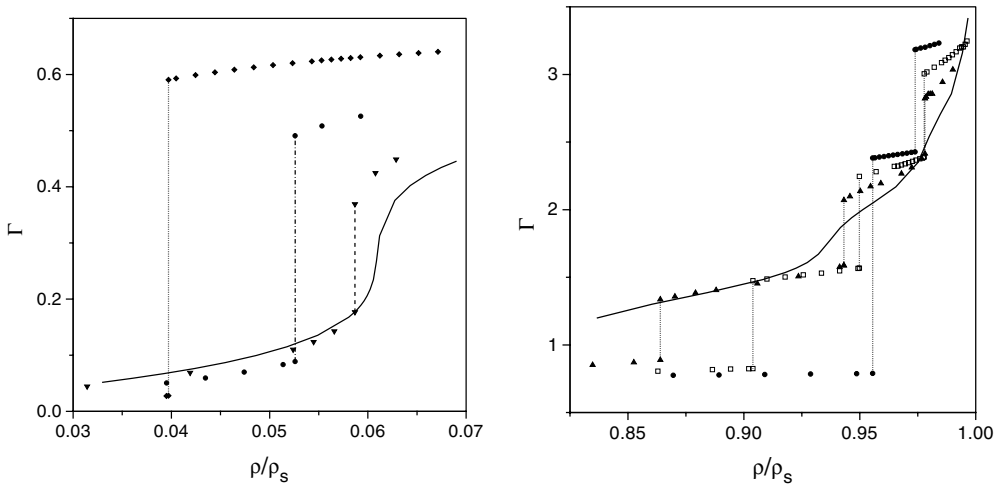

Figure 1. The adsorption isotherm for the two-site, associating model fluid with $\varepsilon_{as} = 8$, adsorbed on the single, solid plane surface (the fluid–wall potential is given by (5) with the following parameters: $\lambda = 5$ and $\varepsilon_{gs} = 10$). In (a) at $T^* = 0.975$, (full curve), $T^* = 0.95$, (triangles), at $T^* = 0.90$, (circles) and $T^* = 0.80$, (diamonds). In (b) at $T^* = 1.1$, (full curve), $T^* = 1.06$, (up triangles), $T^* = 0.975$, (squares) and $T^* = 0.90$ (circles). The low-density part of the isotherms (a) and their high-density (b) describe the first layering transition and subsequent layering transitions, respectively. In both panels the phase transitions are shown by vertical lines.

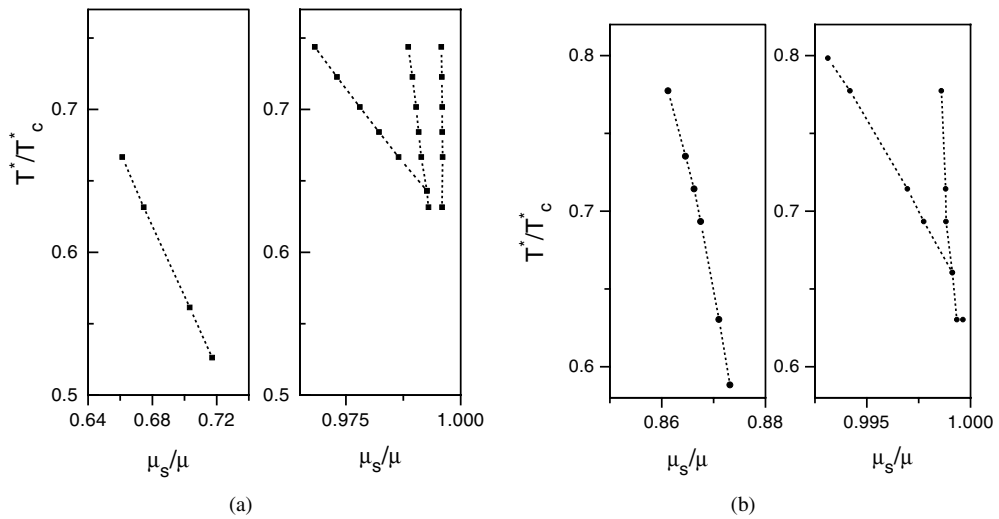

Figure 2. The phase diagrams for a weakly associating (a) and strongly associating (b) fluid in contact with single, plane solid surface, $\varepsilon_{gs} = 10$, $\lambda = 5$, in the form of dependencies of the temperature of a transition on the degree of undersaturation.

first layering transition, whereas figure 1(b) gives an insight into the evolution of the second, third and fourth layering transitions with temperature.

However, a compressed view of the phase behaviour of a weakly associating fluid in contact with solid surface in question is given in figure 2(a) (the chemical potential scale here and in the following is with respect to the chemical potential at saturation, μ_s: the

temperature scale is normalized by the critical temperature of the relevant *bulk* fluid). On the other hand, a similar phase diagram for a strongly associating fluid is shown in figure 2(b). In discussing the results in figure 2(a) it is important to mention the following features. The surface remains wet even at quite low temperatures. The locus of four layering transitions has been well established in the range of temperatures of interest, it becomes more difficult to perform calculations very close to the coexistence and localize precisely higher-order layering transitions which are present according to our calculations. The critical temperature of the first layering transition is substantially depressed with respect to the critical temperature of the bulk model (see the left panel of figure 2(a)). On the other hand, the critical temperatures of the second and following layering transitions are depressed less (see the right panel of figure 2(a)). The branch corresponding to the second layering transition merges with the branch of the third transition such that the number of layering transitions decreases with decreasing temperature. Nevertheless, we can conclude that the solid surface in question belongs either to the class of strong substrates or intermediate substrates in the classification of Pandit *et al* [39]. We were not able to establish the value for the roughening temperature but seemingly trends of behaviour of the critical temperatures for layering transition coincide with those predicted by Pandit *et al* [39] for simple fluids in contact with intermediate-substrate systems.

Similar calculations and analysis have been performed for a strongly associating fluid (figure 2(b)). Again we observed layering transitions, just the first three of them have been localized precisely. It is important to mention that the critical temperatures for layering transitions in this case are higher in reduced units, in comparison with a weakly associating case (cf figure 2(a)). The differences between the critical temperature of the first layering and subsequent transitions is much smaller for a strongly associating case than for a weakly associating fluid. Moreover, the layering transitions are located much closer to the coexistence curve, in comparison with a weakly associating case. All these trends in common serve as a manifestation of the importance of the effects of bonding on the phase behaviour. The trends observed are physically well understood (some of these trends, however for LJ type attractive surfaces, have been discussed in great detail in our previous work [30]). To summarize, the strongly associating fluid feels the confining surface in question again as an intermediate-substrate system. After establishing with what solid surface we are dealing with, we proceed with the results obtained for the fluid model in cylindrical pores.

3.2. Adsorption and phase transitions in cylindrical pores

The essence of the results of our study is given in terms of the phase diagrams. The fluid model is studied at $\varepsilon_{as} = 8$ and $\varepsilon_{as} = 20$ (as in the above). The fluid–pore walls potential is given by (4). We consider two cylindrical pores, namely with $R_c = 2.5$ and $R_c = 4.5$, referred to in the following as a narrow and wide pore, respectively. The phase diagrams for a weakly associating and strongly associating model are given in figures 3(a) and 3(b), respectively. Here, $\langle\rho\rangle = \int \mathrm{d}R\, \rho(R)/R_c^2$, is the average fluid density inside the pore.

Several observations are of interest. First, let us focus on the weakly associating model case. In the narrow pore the phase diagram consists of two branches, one branch describing the first-order layering transition and the second branch describing capillary condensation. In a wide pore, the capillary condensation branch decouples such that the left-hand side of it exists as a branch describing the second layering transition. There is a 'triple' point between the second layering transition and capillary condensation over the entire pore. We observe that the critical temperature of the first layering remains almost unchanged while the pore radius changes. Moreover, the critical temperature of the first layering is almost equal to that evaluated for a single plane solid surface (cf figure 1(a)). The critical temperature of the

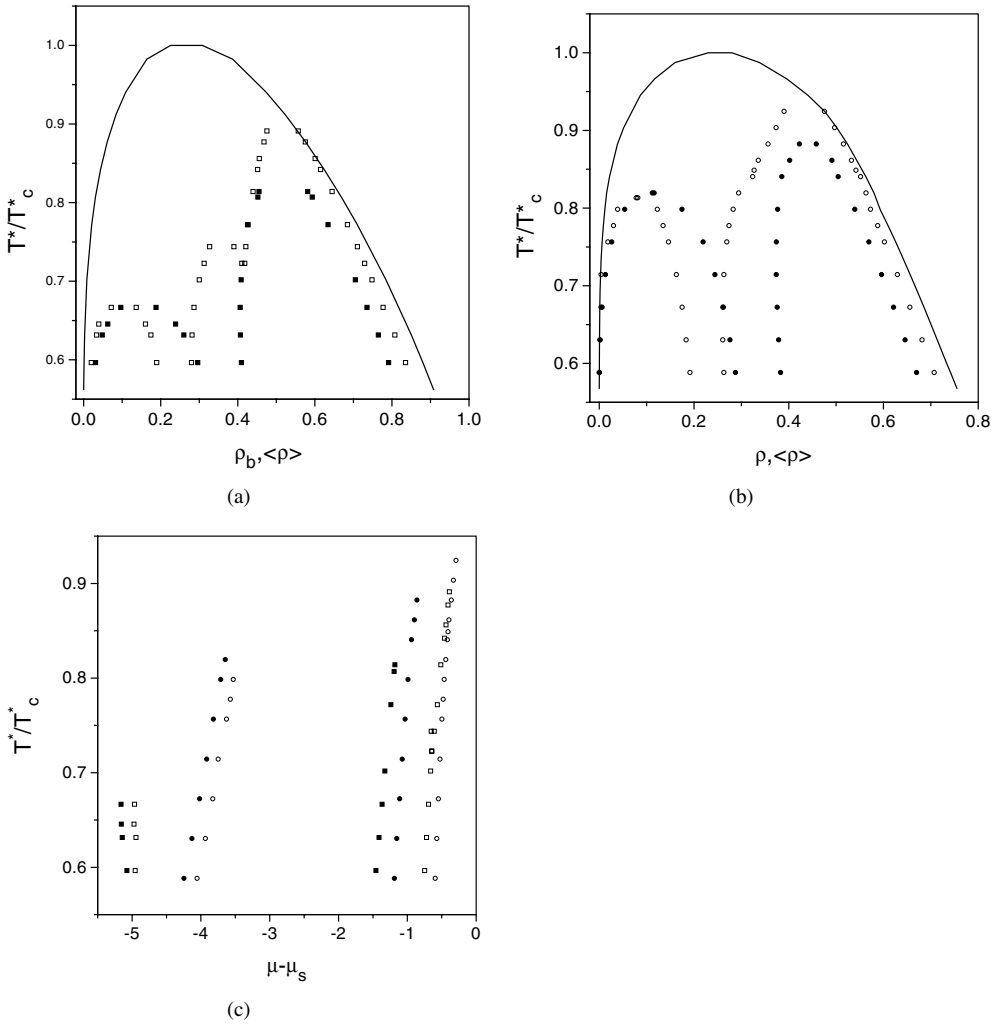

Figure 3. The phase diagrams for a weakly associating (a) and strongly associating (b) fluid adsorbed in a narrow ($D_c = 5$) and wide ($D_c = 9$) cylindrical pore. The phase diagrams are given by the solid and empty symbols for a narrow and wide pore, respectively. (c) is a comparison of the phase diagrams for a weakly and strongly associating fluids in a narrow and wide cylindrical pore (empty symbols, wide pore; solid symbols, narrow pore; squares, weakly associating fluid; circles, strongly associating fluid). For each type of symbol, the branch at higher undersaturation, i.e. at lower values of the chemical potential, corresponds to the layering transition whereas the branch at lower undersaturation is for the capillary condensation.

second layering also remains almost equal to that observed for a single solid surface. The critical temperature for capillary condensation is strongly depressed with respect to the critical temperature of the bulk model. The depression is much stronger in a narrow pore than in a wide pore, as expected. The critical density of the first layering seems to be more influenced by changes of confinement rather than the critical density for capillary condensation for the pores in question.

Now, let us proceed to the case of a strongly associating fluid adsorbed in cylindrical pores. Both phase diagrams shown in figure 3(b) consist of two branches, corresponding to

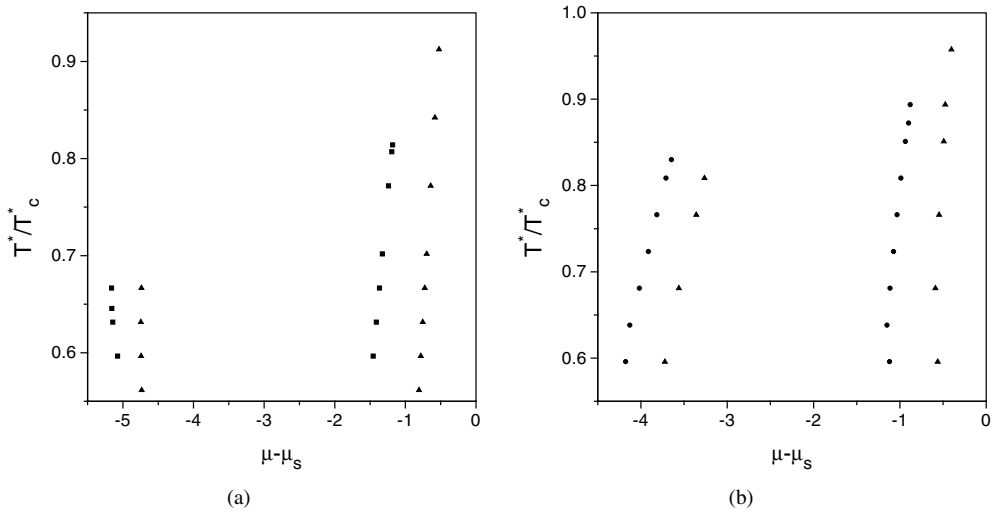

Figure 4. A comparison of the phase diagrams for a weakly associating (a) and strongly associating (b) fluid adsorbed in a narrow slit and cylinder ($D_c = H = 5$) and wide slit and cylinder ($D_c = H = 9$). The phase diagrams are given by solid triangles (slit) and solid squares or circles (cylinder). For each type of symbol, the branch at higher undersaturation, i.e. at lower values of the chemical potential, corresponds to the layering transition whereas the branch at lower undersaturation is for the capillary condensation.

the first layering transition and to capillary condensation, respectively. In a wider pore the left-hand side of the capillary condensation branch is non-monotonous—one would expect the appearance of the second layering transition in a still wider pore. The width of each of the branches is sensitive to confinement: narrower layering branch—wider capillary condensation branch and *vice versa*. Again, the critical density of the first layering seems to be slightly more influenced by confinement rather than the critical density of the condensation branch. However, the critical temperature for the first layering in both pores is higher in comparison to the relevant critical temperature in adsorption on a plane wall. The critical temperatures (in reduced units) for capillary condensation are systematically higher for the strongly associating case than for a weakly associating one. The lower depression of the critical temperature for condensation is due to stronger trends for bonding between fluid species. The stronger the bonding between them the more competitive becomes their interaction with respect to the attraction between the fluid–pore walls. A compressed insight into the phase diagrams trends, supporting our discussion, is given in figure 3(c).

We have performed similar calculations and analysis for the fluid models in question for slit-like pores with a nominal width equal to the diameter of a cylindrical pore. A comparison of the corresponding phase diagrams for a weakly associating and strongly associating fluid is given in figures 4(a) and 4(b), respectively. To summarize this group of results, we would like to mention that the branches which correspond to the layering transition are characterized by very similar critical temperatures. The critical density is more influenced by the shape of confinement. Stronger confinement in the cylinder, in comparison with a slit, yields a lower critical density of transition (i.e. the transition occurs at a lower value of the chemical potential). However, the critical properties of the first layer are mostly determined by the fluid–wall interaction and intrinsic characteristics of the fluid model rather than by confinement. On the other hand, while the trends of the behaviour of the critical density for condensation which are dependent on the geometry of the pore are similar to those observed for the layering transition,

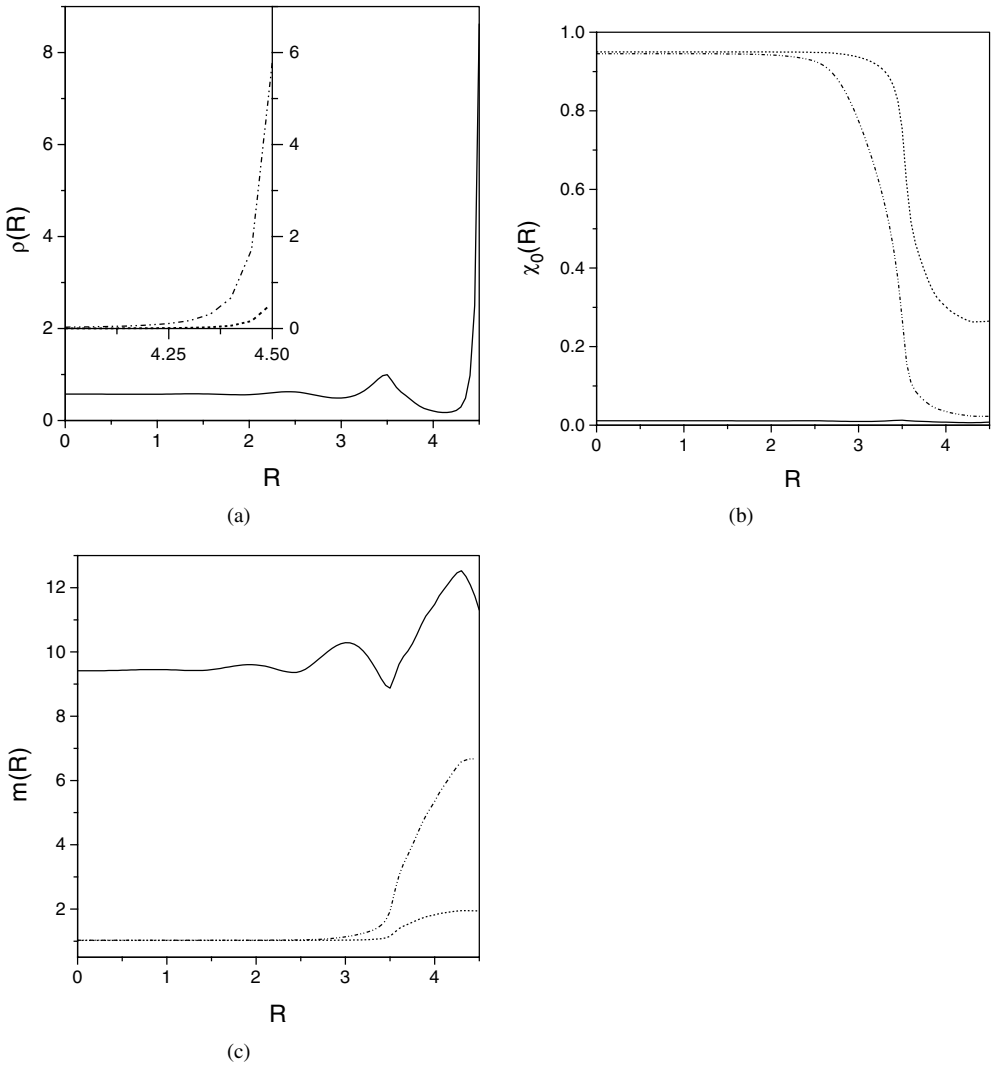

Figure 5. The density profiles (a), the density profiles of unbonded particles, i.e. of monomers (b), and the density profiles for the average chain length (c), before and after capillary condensation. This case is for $T^*/T_c^* = 0.733$ and $\varepsilon_{as} = 8$ for narrow pore ($D_c = H = 5$). The broken curve corresponds to $\rho_b = 0.0965$, the dash–dotted curve to $\rho_b = 0.1880$ and the full curve to $\rho_b = 0.7371$.

the depression of the critical temperature is sensitive to different confinement. Stronger confinement in the cylindrical pore yields a much stronger depleted critical temperature in comparison with the slit-like pore. Higher critical temperatures are observed for a strongly associating fluid in comparison with a weakly associating fluid, as already mentioned.

3.3. Structural properties of the model adsorbed in cylindrical pores

Next, we would like to comment quite briefly about structural changes in the adsorbed chain-forming fluid model occurring when the fluid undergoes a layering transition and

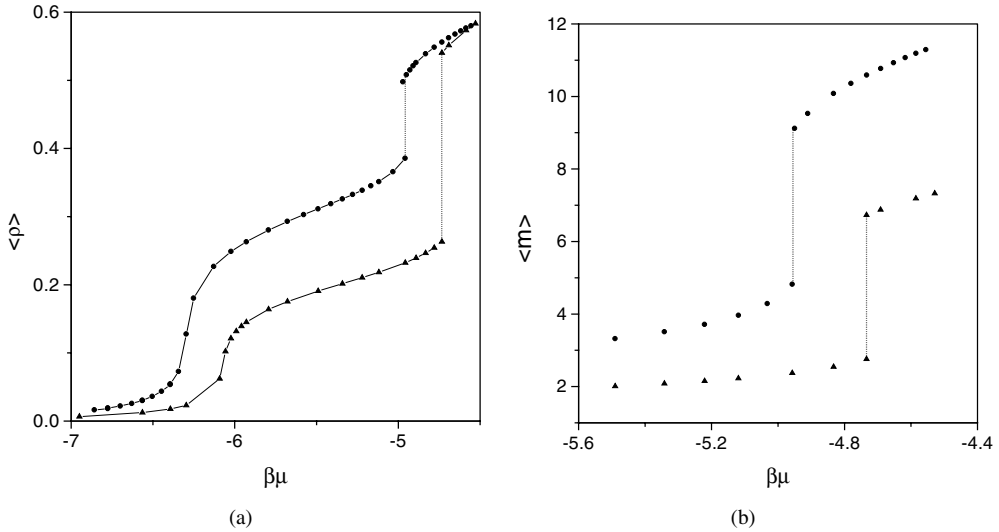

Figure 6. (a) the average density for a strongly associating fluid, at $T^*/T_c^* = 0.84$, in narrow cylindrical (circles) and in slit-like (triangles) pores ($D_c = H = 5$) versus the chemical potential. (b) the average chain length along the isotherms given in (a).

capillary condensation. The density profiles shown in figure 5 are for the strongly associating model, $\varepsilon_{as} = 20$, at $T^*/T_c^* = 0.733$ in a wide cylindrical pore, $D_c = 2R_c = 9$. The figure consists of three panels, in the first one we present the density profile of the fluid species before the layering transition, after the layering transition and after capillary condensation occurred in the entire pore. Due to strong bonding effects the profiles do not exhibit much structure. Filling of the first layer adjacent to the pore wall results in a drastic change of the contact value of the profile, farther from the pore wall, the pore remains almost empty (figure 5(a)). On the other hand, during capillary condensation, the contact value is not changed so drastically, rather the second maximum of the profile develops and simultaneously the density in the entire pore becomes high. The value of the density in the central part of the pore is almost constant, however. One can observe that bonding effects have an essential influence on the fluid structure in the pore. The density profile of the unbonded species, $\chi_0(R) = 1/\chi_A^2(R)$, shown in figure 5(b), is given by using the same nomenclature of lines as in figure 5(a). Before the first layering transition the fraction of the unbonded species is low in the close vicinity of the pore wall but rapidly saturates, to the value of $\approx$0.95. Thus a small fraction of bonded particles is present over the entire pore. After the layering transition these trends of behaviour preserve, with the exception that the region where the fraction of the unbonded species is low extends farther from the pore wall. Finally, after the capillary condensation, the profile of the unbonded species is negligibly small over the entire pore.

The density profile for the average chain length, $m(R) = 1/\chi_A(R)$, is given in figure 5(c). Before and after the layering transition the profile differs from the value attained in the central part of the pore only in the close vicinity of the pore wall. In the central part of the pore in these two cases the average chain length is very slightly larger than unity. After the layering transition chains consisting of approximately six monomers are formed in the layer adjacent to the pore wall. After the capillary condensation, the average chain length in the central part of the pore is high—chains involve more than nine monomers on average. The profile oscillates in the vicinity of the pore wall, close to the wall chains consisting of approximately twelve monomers are formed. However, the small depletion of the profile at contact manifests steric

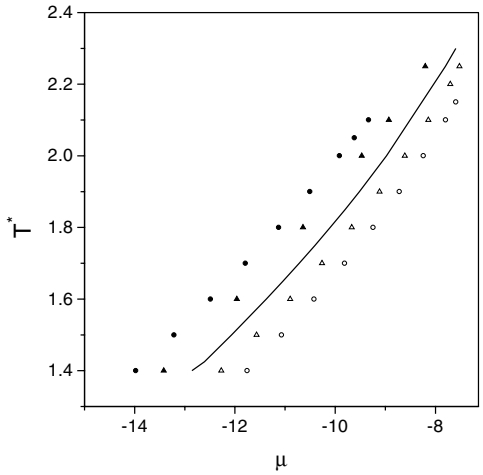

Figure 7. The phase diagram for capillary evaporation (empty symbols) and for capillary condensation (solid symbols) for a narrow pore ($D_c = H = 5$) for a strongly associating fluid, $\varepsilon_{as} = 20$, (cylindrical pore, circles and slit-like pore, triangles). The full curve corresponds to the bulk liquid–vapour transition.

restriction due to the pore wall curvature. Presumably, chains prefer parallel orientation with respect to the pore wall as follows from the period of oscillations.

In general, the formation of chains via the association of monomers is quite sensitive to the shape of confinement. To prove this, we present in figure 6(a) the isotherms of the average densities for the narrow cylindrical pore, $D_c = 5$, and for a slit-like pore with $H = 5$. Both isotherms were calculated at a temperature equally distanced from the critical temperature of the bulk strongly associating fluid, $T^*/T_c^* = 0.84$. The value for the average chain length on the chemical potential in both cases is shown in figure 6(b). We observe that after capillary condensation the average density in both pores is almost equal. However, the composition, as reflected in the values of $\langle m \rangle$, is quite different. The average chain length in the fluid confined to the cylindrical pore, in equilibrium with the fluid confined to the slit-like pore of comparable width, is essentially higher than in the slit-like pore.

3.4. Capillary evaporation in the cylindrical and slit-like pores

Our final remarks concern the phenomenon of capillary evaporation in the cylindrical and slit-like pores. The phase diagram for capillary evaporation for associating fluids has not been studied so far. In order to investigate trends of capillary evaporation in both cylindrical and slit-like pores, we have switched off the attractive fluid–wall interaction in both cases, only the impermeability of the pore walls have remained. One example of the phase diagram for evaporation together with capillary condensation in a narrow pore ($D_c = 5$ and $H = 5$) for a strongly associating fluid, $\varepsilon_{as} = 20$, is shown in figure 7. The branches corresponding to condensation and evaporation are almost equidistant from the bulk liquid–vapour transition line both for the cylindrical and for the slit-like pore. The critical temperature for evaporation is depressed to the same extent, as that for condensation in the case of the slit-like pore. In the case of a cylindrical pore, the critical temperature for evaporation is depressed slightly less than for condensation. Nevertheless, branches corresponding to condensation and to evaporation in the cylindrical pore are more separated, with respect to the transition in the bulk system, than the branches corresponding to the transitions in the slit-like pore. This behaviour

reflects the stronger confinement effects in the cylindrical pore on the critical phenomena in question.

4. Conclusions

We have investigated the adsorption and phase transitions of the two-site associating fluid model in cylindrical pores. The wetting properties of the solid surface forming the pore walls have been characterized. In addition, we have performed several calculations for slit-like pores, for a comparison with the results for cylindrical pores, and elucidate the effects of the pore geometry on the adsorption and critical phenomena. In all the cases, the fluid wets the surface up to low temperatures, such that the pore walls can be classified as strongly or intermediate substrates. We have established that capillary condensation of the model associating fluid in question is preceded by one or two layering transitions dependent on the pore width, and on the association energy between monomers. The dense layer adjacent to the pore wall consists of highly bonded species, whereas in the dilute phases free monomers prevail. We have observed that the critical temperature of the first layering transition, both in the cylindrical and in slit-like pores, almost coincides with that for the same fluid adsorbed on the plane substrate. In contrast, the critical temperature for capillary condensation is very dependent on the geometry and volume of the pores. This is understandable, because with the decreasing radius of a cylindrical pore, the confined fluid reduces to a one-dimensional system, and all the phase transitions become suppressed, see e.g. [40]. Moreover, the adsorbed strongly associating fluid exhibits weaker trends for the depression of the critical temperature than a weakly associating fluid. The stronger association between monomers in the adsorbed fluid also results in a smaller difference between the critical temperatures for layering and capillary condensation transitions. The critical temperature for capillary evaporation in cylindrical and slit-like pores exhibits depression of the same order of magnitude as the capillary condensation with respect to the critical temperature of the bulk fluid. Our results for the adsorption of a weakly associating model are in qualitative agreement with those obtained in previous works for non-associating fluids in cylindrical pores [31, 32]. Some differences and some new features can be attributed to the different modelling of the non-associative interactions between fluid species, to different energetic parameters of attraction and different decay of the fluid–wall attraction. However, the effects of association between fluid species clearly follow from the results presented in our study. Moreover, similar investigations performed for one-site and four-site LJ associating model fluids have convinced us that the trends discussed in this work are of more general validity.

Our expectation is that the results of this study would be helpful for further theoretical developments in the spirit of combining the SAFT and density functional approaches. An adjustment of the parameters of the model and pore walls surfaces would also be necessary in a future study. However, it is most important for future developments to consider a density functional approach in order to allow mixtures of fluid species to be dealt with adequately. Hopefully, the density functional approach of Rosenfeld, Kierlik and Rosinberg would be of much interest. Our principal intention in this work was, however, to elucidate the effects of the pore geometry on adsorption and phase transitions in associating fluids at a basic level.

Acknowledgments

This project was supported in part by the National Council for Science and Technology (CONACyT) under grant no 25301-E and by Silicon Graphics Inc. The work of SS was supported by the project no 3T09A 08216 of the KBN of Poland.

References

[1] Nicholson D and Parsonage N D 1983 *Computer Simulation and the Statistical Mechanics of Adsorption* (New York: Academic)
[2] Schoen M 1993 *Computer Simulation of Condensed Phases in Complex Geometries (Lecture Notes in Physics)* (Berlin: Springer)
[3] Schoen M 2000 *Computational Methods in Surface and Colloid Science* ed M Borowko (New York: Marcel Dekker) ch 1
[4] Wertheim M S 1984 *J. Stat. Phys.* **35** 19
Wertheim M S 1984 *J. Stat. Phys.* **35** 35
[5] Wertheim M S 1986 *J. Stat. Phys.* **42** 459
Wertheim M S 1986 *J. Stat. Phys.* **42** 477
[6] Wertheim M S 1986 *J. Chem. Phys.* **85** 2929
[7] Wertheim M S 1987 *J. Chem. Phys.* **87** 7323
[8] Jackson G, Chapman W G and Gubbins K E 1988 *Molec. Phys.* **65** 1
Jackson G, Chapman W G and Gubbins K E 1988 *Molec. Phys.* **65** 1057
[9] Chapman W G 1990 *J. Chem. Phys.* **93** 4299
[10] Chang J and Sandler S I 1995 *J. Chem. Phys.* **102** 437
[11] Ghonasgi D and Chapman W G 1993 *Molec. Phys.* **79** 291
[12] Nezbeda I and Slovak J 1997 *Molec. Phys.* **90** 353
[13] Chapman W G, Gubbins K E, Jackson G and Radosz M 1990 *Ind. Eng. Chem. Res.* **29** 1709
[14] Kraska T and Gubbins K E 1996 *Ind. Eng. Chem. Res.* **35** 4727
[15] Galindo A, Whitehead P J, Jackson G and Burgess A N 1998 *J. Phys. Chem.* **100** 6781
[16] Galindo A, Gil-Villegas A, Whitehead P J, Jackson G and Burgess A N 1998 *J. Phys. Chem.* **102** 7632
[17] Holovko M F and Vakarin E 1995 *Molec. Phys.* **85** 1057
[18] Pizio O, Henderson D and Sokolowski S 1995 *J. Phys. Chem.* **99** 2408
[19] Trokhymchuk A, Pizio O, Henderson D and Sokolowski S 1996 *Chem. Phys. Lett.* **262** 33
[20] Henderson D, Pizio O, Sokolowski S and Trokhymchuk A 1997 *Physica* A **244** 147
[21] Evans R 1992 *Fundamentals of Inhomogeneous Fluids* ed D Henderson (New York: Marcel Dekker) ch 3
[22] Henderson D 1992 *Fundamentals of Inhomogeneous Fluids* ed D Henderson (New York: Marcel Dekker) ch 2
[23] Rocken P, Somoza A, Tarazona P and Findenegg G 1998 *J. Chem. Phys.* **108** 8689
[24] Gac W, Patrykiejew A and Sokolowski S 1994 *Surf. Sci.* **306** 434
[25] Segura C J, Chapman W G and Shukla K 1997 *Molec. Phys.* **90** 759
[26] Segura C J, Vakarin E V, Chapman W G and Holovko M F 1998 *J. Chem. Phys.* **108** 4837
[27] Patrykiejew A and Sokolowski S 1999 *J. Phys. Chem.* B **103** 4466
[28] Huerta A, Sokolowski S and Pizio O 1999 *Molec. Phys* **97** 919
[29] Huerta A, Sokolowski S and Pizio O 2000 *J. Chem. Phys.* **112** 4286
[30] Millan Malo B, Huerta A, Sokolowski S and Pizio O 2000 *J. Phys. Chem.* B **104** 7756
[31] Evans R, Marconi M B and Tarazona P 1986 *J. Chem. Soc. Faraday Trans. 2* **82** 1763
[32] Evans, R and Ball P C 1988 *J. Chem. Phys.* **89** 4412
[33] Weeks D, Chandler D and Andersen H C 1997 *J. Chem. Phys.* **54** 5237
[34] Tarazona P 1985 *Phys. Rev.* A **31** 2672
Tarazona P 1985 *Phys. Rev.* A **32** 3148 (Erratum)
[35] Segura C and Chapman W G 1995 *Molec. Phys.* **86** 415
[36] Johnson J K and Gubbins K E 1992 *Molec. Phys.* **77** 1033
[37] Walsh J M and Gubbins K E 1993 *Molec. Phys.* **80** 65
[38] Müller E A and Gubbins K E 1995 *Ind. Eng. Chem Res.* **34** 3662
[39] Pandit R, Schick M and Wortis M 1982 *Phys. Rev.* E **26** 5112
[40] Balbuena P, Gubbins K E, 1994 *Stud. Surf. Sci. Catal.* **87** 41